Acta Biomaterialia 7 (2011) 2873–2882

Contents lists available at ScienceDirect

Acta Biomaterialia

journal homepage: www.elsevier.com/locate/actabiomat

Synthesis of nanocarriers with remote magnetic drug release control and enhanced drug delivery for intracellular targeting of cancer cells

W.-L. Tung, S.-H. Hu, D.-M. Liu *

Department of Materials Science and Engineering, National Chiao Tung University, 1001 Ta Hsueh Road, Hsinchu 300, Taiwan

ARTICLE INFO

Article history:
Received 10 November 2010
Received in revised form 25 February 2011
Accepted 16 March 2011
Available online 23 March 2011

Keywords:
Magnetic nanoparticles
Controlled release
Drug delivery
Targeting
Cancer

ABSTRACT

Nanotherapeutic strategy is well recognized as the therapeutic approach of the future. Numerous reports have demonstrated the use of nanoparticulate drug carriers for the development of targeted nanotherapeutics by, for instance, incorporation of a moiety that specifically targets certain diseased cells. However, systematic investigation of this aspect has been inadequate, especially with regard to nanosystems with remotely controlled drug delivery. The authors previously designed a magnetic-responsive core–shell drug delivery nanosystem which proved to be technically feasible in vitro. In the present study, this nanosystem is modified for targeted delivery of an anticancer agent (encapsulated camptothecin (CPT)) to cancer cells overexpressing epithelial growth factor receptor (EGFR) with accurate intracellular drug release. The endocytosis of the nanocarriers by cancer cells, the pathway of cellular uptake and the subsequent intracellular controlled drug delivery were systematically investigated. It was found that the modified nanocarriers showed reasonably high drug load efficiency for CPT and a high uptake rate by cancer cells overexpressing EGFR through clathrin-mediated endocytosis. The intracellular release of the CPT molecules via an external magnetic stimulus proved to be technically successful and ensured much higher therapeutic efficacy than that obtained with the free drug. This study employs multiple functions for nanotherapeutic treatment of specific target cells, i.e. cell-specific targeting, controlled cellular endocytosis and magnetic-responsive intracellular drug release.

1. Introduction

One of the main goals of nanomedicine is to develop a nanocarrier that can selectively deliver anticancer drugs to target tumors and affect as few healthy cells as possible. The past decades of outstanding progress in fundamental cancer biology have not translated into comparable advances in clinical cancer chemotherapy. Traditional liposomal drug carriers are limited by low drug encapsulation efficiency (EE), poor storage stability, rapid clearance from the blood stream, non-specific uptake by the mononuclear phagocytic system, poor control over release of the drug from the liposome and rapid drug loss profiles in vivo [1,2]. By integrating the explosive developments of nanotechnology and oncology in drug delivery, many types of nanocarrier have the potential for offering solutions for several of these problems [3]. For example, some targeting molecules attached to nanocarriers, such as antibodies, peptides, ligands or nucleic acids, further enhance the recognition and internalization of the carriers by target sites such as human epidermal growth factor receptor-2 (HER-2) [4–6] and folic acid receptor [7–9]. Moreover, most drug-containing nanoparticles achieve accumulation in tumor tissues through enhanced permeation and retention (EPR) [10,11], resulting in a several-fold increment of drug concentrations in solid tumors relative to those obtained with free drugs [12]. The next generation of nanoparticle-based research is directed at the consolidation of functions into strategically engineered multifunctional systems which may ultimately facilitate the realization of personalized therapy. Such multiplexed nanoparticles may be aimed at integrating therapeutic, diagnostic or monitoring components in a synergistic fashion to achieve a more potent target response and to eliminate cancer cells with minimal side effects through selective drug targeting and treatment monitoring in real time [13]. The magnetically sensitive iron oxide nanoparticle is an outstanding candidate for multifunctional systems as a contrast agent, drug carrier or a combined function, or for assembly into a device-like carrier. Such magnetic nanoparticles can be further functionalized through surface modification or combination with functional moieties on their surface, as widely highlighted in a variety of biomedical applications, including drug/gene delivery [14–17], bioseparation [18], magnetic resonance imaging [19,20] and hyperthermia therapy [21]. However, reports addressing key issues between such magnetic sensitive nanosystems and the biological environment, such as cellular uptake, cell-specific targeting, cellular internalization and

* Corresponding author. Tel.: +886 3 5712121x55391; fax: +886 3 5725490.
E-mail address: deanmo_liu@yahoo.ca (D.-M. Liu).

1742-7061/$ - see front matter © 2011 Acta Materialia Inc. Published by Elsevier Ltd. All rights reserved.
doi:10.1016/j.actbio.2011.03.021

intracellular drug delivery, are most desirable. A deeper understanding of such nanosystem–cell interaction is expected to encourage the development of a better nanotherapeutic strategy for targeted diseases such as malignant tumors. However, to improve the therapeutic efficacy of the nanoparticle-based drug delivery system, it is critically important to understand the physicochemical properties and the role of the cancer-cell phenotype in the adhesion [22] and uptake of the carrier and intracellular trafficking. To date, several reports have discussed the internalization of nanoparticles into target cells by endocytic pathways in terms of their size, concentration and biological behavior [23–25].

In a previous study, a novel drug delivery nanosystem was designed and constructed by self-assembly of iron oxide (SAIO) nanoparticles in the presence of polyvinyl alcohol (PVA), followed by coating with a thin layer of silica shell for controlled drug release via an external magnetic stimulus; ibuprofen (IBU) was employed as a model molecule [26]. However, IBU did not show any therapeutic effect for cancer in real time, and the study did not discuss the interaction between drug delivery nanosystem and organisms in earlier works. In the present study, this nanosystem was equipped for intracellular delivery of targeted anticancer drugs. The chemotherapeutic drug, camptothecin (CPT), a relatively water-insoluble compound, was employed, encapsulated in the magnetic core and covered with an ultra-thin silica shell (hereafter termed CPT-SAIO@SiO_2). In addition, poorly water-soluble drugs are difficult to develop as a conventional formula [27], and thus SAIO@SiO_2 is an interesting candidate for a solution to this problem. The thin silica shell was designed as a physical barrier to eliminate undesirable drug leakage, so that for clinical use a better and more timely manageable dosage of the drug could be delivered on reaching the target sites. Then, use of an external magnetic stimulus allows a pulse-type drug release to be readily achieved in a realtime responsive manner without undesirable delays in dosing accuracy. Furthermore, the CPT-SAIO@SiO_2 was modified using a specific ligand, i.e. anti-EGFR (epithelial growth factor receptor), for targeting the EGF receptor which has elevated expression in non-small-cell lung cancer [28]. The behavior of cells following incubation with CPT-SAIO@SiO_2 nanocarriers and exposure to a magnetic field was also monitored. In addition, the cellular uptake efficiency and the internalization fate of these novel cell-targeting CPT-SAIO@SiO_2 nanocarriers were systematically examined. Anti-EGFR conjugated CPT-SAIO@SiO_2 nanocarriers were successfully designed for selective and effective intracellular delivery to the A549 cell line. It was not only internalized in the right population of cells, but also showed controllability for drug release from the system.

2. Materials and methods

2.1. Synthesis of magnetic nanoparticles

The processes of synthesis were developed by Sun et al. [29]. Five-nanometer iron oxide nanoparticles were mixed with 2 mmol $Fe(acac)_3$, 10 mmol 1,2-hexadecanediol, 6 mmol dodecanoic acid and 6 mmol dodecylamine. The mixture were dissolved in 20 ml benzyl ether and refluxed in 200 °C for 30 min under a flow of nitrogen situation, and then heated to 300 °C for another 1 h. After cooling, the product was collected by centrifugation at 6000 rpm for 10 min and then washed four times with excess ethanol.

2.2. Synthesis of SAIO@SiO_2 nanocarriers

The self-assembled iron oxide nanoparticles were prepared by taking iron oxide nanoparticles dispersed in chloroform to form an oil phase and adding 2% PVA aqueous solution as a polymer binder. The mixture was emulsified by ultrasonication, then heated to evaporate the organic solvent. After the solvent had been removed, the mixture was washed in deionized water (DI water) and collected. The precipitates were redispersed in water, and are hereafter termed SAIO. The silica shells were coated on the SAIO nanospheres by modifying the Stöber method, where SAIO were dispersed in absolute alcohol and added dropwise to tetraethylorthosilicate (TEOS). Then 33% NH_4OH was added to the mixture and stirred for 12 h. After hydrolysis and condensation, it was washed with DI water and redispersed in water, termed SAIO@SiO_2 hereafter.

2.3. Anti-EGFR modifications

First, 5 mg SAIO were dispersed in 4 ml of 99.5% ethanol, 40 μl TEOS and 40 μl ethanolic 3-aminopropyltrimethoxysilane (APTMS) was slowly added to the mixture separately and stirred for 30 min. Then, 0.1 ml of 33% NH_4OH was added to the solution and stirred for 12 h. After hydrolysis and condensation, the amino groups were exposed on SAIO@SiO_2 nanocarriers. Then, 20 μl anti-EGFR was well mixed with amino group exposed SAIO@SiO_2 nanocarriers and incubated at 4 °C for 2 h, and 50 μl 0.1% 1-ethyl-3-[3-dimethylaminopropyl]carbodiimide hydrochloride (EDC) was added to the mixture and magnetically stirred for 4 h. Finally, the unreacted chemicals were removed by rinsing with DI water, termed hereafter SAIO@SiO_2@AE, anti-EGFR conjugated on SAIO@SiO_2 nanocarriers. In addition, the grafted efficiency of anti-EGFR was measured by UV–Vis spectrometer at a wavelength of 275 nm.

2.4. Drug loading and release

Drug-loaded nanocarriers were prepared by dissolving 0.25 mg ml^{-1} CPT ((S)-(+)-CPT, ~95%, Sigma) in chloroform with iron oxide nanoparticles in an oil phase. CPT, iron oxide nanoparticles and PVA are components forming a core phase, i.e. SAIO, before ultrasonication, and silica shell was also applied on SAIO to form drug-loaded SAIO@SiO_2 (termed CPT-SAIO@SiO_2). Then, CPT-SAIO@SiO_2 was collected by centrifugation, and free CPT, and the supernatant was removed. Before the drug release test, the CPT-SAIO@SiO_2 nanocarriers were centrifuged and re-suspended in Dulbecco's modified Eagle's medium (DMEM). CPT loaded in the nanocarriers was quantified using a UV–Vis spectrometer (SP-8001, Metertech Inc.) at a wavelength of 366 nm, a characteristic absorption band of CPT. To measure the concentration of drug released, the dispersed nanocarriers were separated by centrifugation and taken out of the clear solution for estimation. The EE of the drug in the nanocarriers was calculated as follow: $EE(\%) = A/B \times 100\%$, where A is defined as the amount of CPT released completely from the nanocarriers, and B is the total amount of CPT added in the process.

2.5. Cell culture

Human lung adenocarcinoma cell line A549 and human breast adenocarcinoma cell line MCF7 were obtained from the American Type Culture Collection. Both were grown in DMEM and supplemented with 10% fetal bovine serum and 1% penicillin/streptomycin at 37 °C in a 5% CO_2-humidified atmosphere.

2.6. Determination of cellular uptake by flow cytometry

In order to estimate the cellular uptake of the nanocarriers, green-emitting fluorescein dye was attached to the SAIO@SiO_2 nanocarriers (FITC-SAIO@SiO_2) for the study. First, fluorescein isothiocyanate (FITC) was mixed with ethanolic 3-APTMS solution for 24 h at room temperature to form *N*-1-(3-trimethoxysilylpropyl)-*N*-fluoresceyl thiourea (FITC-APTMS). The cellular uptake

quantity of the nanocarriers was confirmed by flow cytometry. The cells were plated 2×10^5 in 6-well plates and grown to 80% confluence. They were then incubated with FITC-SAIO@SiO_2 or FITC-SAIO@SiO_2@AE particles for different periods, and then washed with phosphate buffered saline (PBS, pH 7.4) three times to remove the nanocarriers that did not enter the cells. The cells were harvested by trypsin–EDTA and re-suspended in medium for subsequent analysis with a flow cytometer by accumulating 10,000 events, and were analyzed using CELLQUEST® software.

2.7. Immunofluorescence and confocal microscopic analysis

Cells were seeded and grown on glass coverslips for 24 h and then treated with FITC-SAIO@SiO_2 or FITC-SAIO@SiO_2@AE particles for 2 h. Afterwards, they were washed in ice-cold PBS and fixed for 15 min with 3% formaldehyde, and permeabilization was performed with 0.1% Triton X-100 in PBS for another 15 min. Then, the cells were blocked for non-specific binding with 1% BSA in PBS, and incubated with primary antibodies against mouse clathrin (1:100 dilution in PBS) for 1 h, washed and then incubated with secondary antibodies conjugated to Alexa Fluor 594 (1:100 in 1% BSA/PBS). Cells were subsequently washed three times in PBS and then stained with DAPI dye (1 μg ml^{-1}) for 10 min. Finally, they were mounted on fresh glass slides with mounting solution (Dako) and observed using confocal microscopy. To label late endosome or lysosome of cells using LysoTracker®, Red Lysosomal Probe, similar to foregoing, A549 cells was incubated with probe-containing medium (50 nM) for 30 min at 37 °C. The cells were rapidly washed with ice-cold PBS and fixed and mounted. Samples were then viewed on a fluorescence microscope.

2.8. Endocytosis pathway analysis

A549 cells were seeded for 24 h in 6-well plates and incubated for 30 min with inhibitors. The optimized inhibitor concentrations were used as follows: cytochalasin D (CytD, 3 μg ml^{-1}); chlorpromazine (CPZ, 6.5 μg ml^{-1}), genistein (50 μg ml^{-1}), methyl-β-cyclodextrin (MβC, 75 μg ml^{-1}) and nocodazole (10 μg ml^{-1}). Later, FITC-SAIO@SiO_2 or FITC-SAIO@SiO_2@AE nanocarriers were treated with A549 for 2 h. Subsequently, the cells were washed three times with PBS and harvested for analysis by flow cytometry. Cellular uptake (%) on A549 was calculated by comparison with that in the absence of inhibitor (100%, control) for both SAIO@SiO_2 and SAIO@SiO_2@AE nanocarriers.

2.9. Effect of magnetic field stimulus

A549 cells were treated with SAIO@SiO_2 or CPT-SAIO@SiO_2@AE nanocarriers for 6 h, and then samples were placed into the coil of HFMF apparatus stimulated by high frequency magnetic field (HFMF, 2.5 kA m^{-1}, 50 kHz) for different durations. Subsequently, cells were incubated for 18 h, and then the anticancer effect was measured by MTT assay. Briefly, the cells were harvested in the log phase growth stage and seeded in 96-well plates, then treated with nanocarriers for 24 h. After that, the cultures were incubated with MTT reagent for 4 h, and the absorbance was monitored on an ELISA reader at a wavelength of 570 nm. Cell viability was determined by comparison with untreated cells and calculated according to the following equation: cell viability (%) = (A_{sample}/$A_{control}$) × 100%.

3. Results and discussion

3.1. Morphological observation of SAIO@SiO_2 nanocarriers

Experimental observation showed that the CPT-SAIO@SiO_2 nanocarriers exhibit a spherical geometry with an average particle diameter of 100 nm (Fig. 1a). The iron oxide nanoparticles ~5 nm in diameter were dispersed relatively uniformly within the core phase of the nanocarriers, while the PVA was employed as a binder to stabilize the iron oxide nanoparticles in position. A thin silica shell coating on the nanocarrriers was prepared by hydrolysis and condensation reactions of TEOS on the surface of the core phase (Fig. 1b). Fig. 1c shows a representative image of CPT-SAIO@SiO_2@AE, which has an average size of 102 nm diameter with no significant difference compared with the size of CPT-SAIO@SiO_2. The silica formed a dense shell ~5 nm thick, uniformly deposited over the entire surface of the core, which is believed to play the role of a physical barrier to reduce undesired release, to a certain extent, e.g. free diffusion, of drug before reaching a targeted disease site and, more plausibly, rendering a potential benefit to minimize side effects due to drug toxicity. In the meantime, the silica layer may also protect the active/therapeutic agents in the core from unwanted or unexpected environmental attack, such as oxidation, acidic/basic reactions, enzymatic digestion, etc. Both the intrinsic hydrophilicity and the protective nature of the silica shell makes the nanocarrier an outstanding candidate for a drug delivery system. In addition, both the SAIO and SAIO@SiO_2 nanoparticles showed excellent dispersion characteristics in the liquid media, i.e. PBS and DMEM (cell culture medium) solutions, for a duration as long as 4 weeks, which suggests that they are potential drug carriers for practical uses, such as administration of injections.

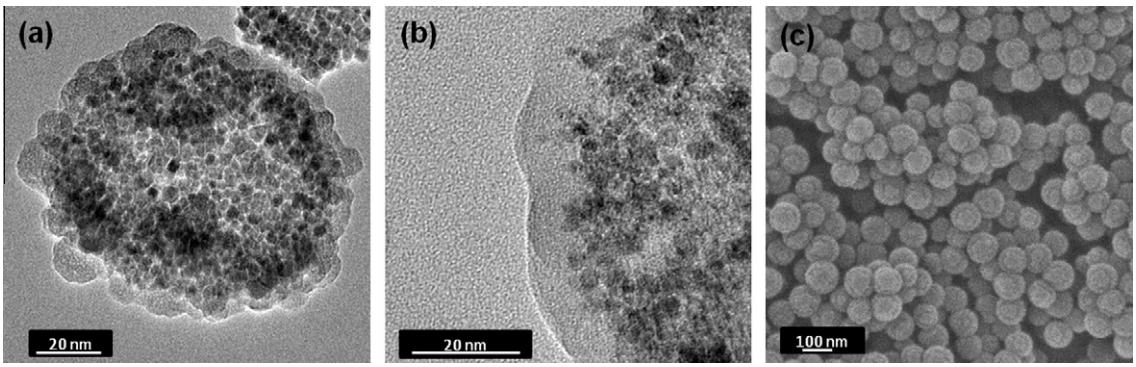

Fig. 1. TEM images of (a) and (b) CPT loaded self-assembled iron oxide/silica core–shell (CPT-SAIO@SiO_2) nanocarriers, and (c) SEM image of CPT-SAIO@SiO_2@AE nanocarriers.

3.2. Encapsulation and release of CPT

Encapsulation efficiency was measured to be 68% for the SAIO nanoparticles by comparison with the amount of the CPT left in the solution after the encapsulation process was completed. However, EE was decreased to a level of ~42% for the SAIO@SiO_2 nanocarriers. This reduction in efficiency is due to the CPT-containing SAIO nanoparticles experiencing a number of washing and centrifugation steps in order to form a thin silica shell covering the SAIO nanoparticles, forming SAIO@SiO_2 nanocarriers. The EE of SAIO@SiO_2@AE is ~38%, believed to be due to the multiple steps of preparation. However, such a loss can be minimized by optimization of the preparation procedure, which is not emphasized in the current study.

Fig. 2a shows the cumulative drug release of the SAIO nanoparticles and SAIO@SiO_2 nanocarriers in DMEM buffer solutions. A burst-like profile to a level of 40% of the drug was monitored in the first 20 min of release for the CPT-containing SAIO nanocarriers, and followed by sustained release to ~48% of the drug for 60 min. The rate of drug release reduced during the next 40 min, believed to be due to the solubility of the hydrophobic drug. The thin silica shell acting as a physical barrier effectively restricts the outward diffusion of the CPT to a considerable extent. It is reasonable to ensure that zero release by free diffusion of the CPT from the nanocarriers can be achieved for a thicker silica layer.

However, the drug was released at only ~6% for a 1-h period for the CPT-SAIO@SiO_2 nanocarriers. Upon closer examination of the release profile for the CPT-SAIO@SiO_2 nanocarriers in Fig. 2a, an amount of ~5% was achieved in the first 5 min, followed by a plateau profile to ~6% for another 55 min of release. This finding indicates that most of the released CPT may be originating from surface desorption from the SAIO@SiO_2 nanocarriers in the preparation process. After desorption from the surface, the CPT is largely inhibited from further diffusion by the silica shell. However, it is also reasonable to ensure that zero release by free diffusion of the CPT from the CPT-SAIO@SiO_2 nanocarriers can be achieved for a thicker silica shell.

This drug elution study clearly indicates that the silica shell, albeit as thin as 5 nm, acts as an effective barrier, which prevents the CPT molecules to a considerable extent from free diffusion. This finding also suggests that the ultrathin silica shell is structurally compact, with full coverage over the entire surface of the SAIO core, as evidenced in Fig. 1b, indicating a highly compatible interface between the silica and core phase. In comparison with these two drug carriers, the addition of an ultrathin silica shell is apparently highly capable of achieving a relatively slow release pattern, which offers the advantages of preserving and protecting the drug molecules in the CPT-SAIO@SiO_2 nanocarrier.

3.3. Magnetically induced CPT release

Under magnetic stimulus, the release profile of CPT for the SAIO@SiO_2 nanocarriers in different eluting media is demonstrated in Fig. 2b and c, where a significant increase in the release profile was detected through DMEM media, compared with those without stimulus (Fig. 2a). This suggests that the rate of drug diffusion was considerably increased upon magnetic stimulus, which, as suggested in a previous study [26,30], is due to thermally induced disruption of the nanostructure of the carriers.

The release behavior of CPT in DMEM buffer is shown in Fig. 2b, where CPT released to an amount of ~18% over a 60-min elution was detected for 0.5-min and 1-min periods of stimulus, while an increment to 40% over the same 60-min elution was detected after the nanocarrier was subjecting to a 2-min stimulus at the very beginning of the elution test. This observation indicates a more extensive thermally induced diffusion and/or dissolution of the CPT and, in the meantime, nanostructural disruption upon a longer-period magnetic stimulus. In comparison with Fig. 2a, a much higher, by four to six times, release amount was obviously

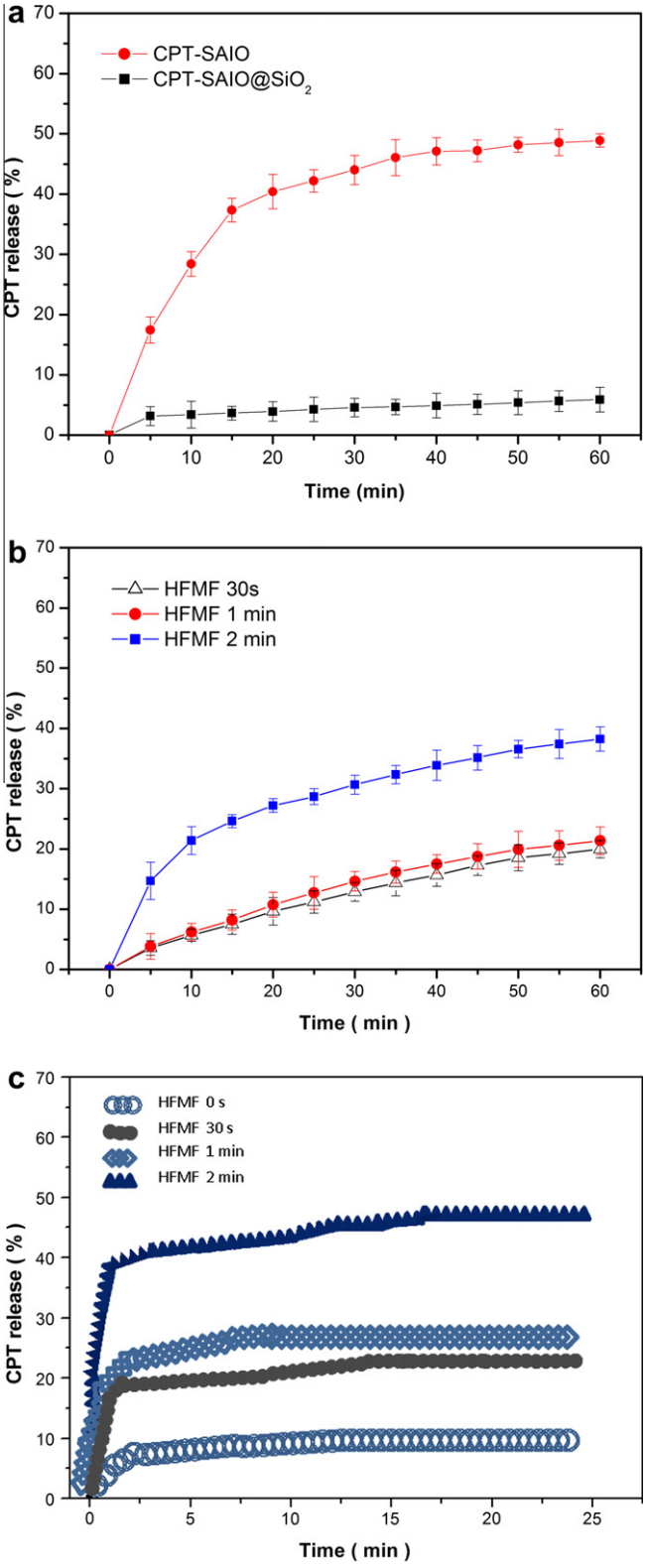

Fig. 2. Cumulative drug release of SAIO and SAIO@SiO_2 nanocarriers, (a) without magnetic field stimulus. (b) Drug release profiles of CPT from CPT-SAIO@SiO_2 nanocarriers were triggered by different periods of magnetic stimulus in DMEM; (c) the drug release profile monitored for 24 h.

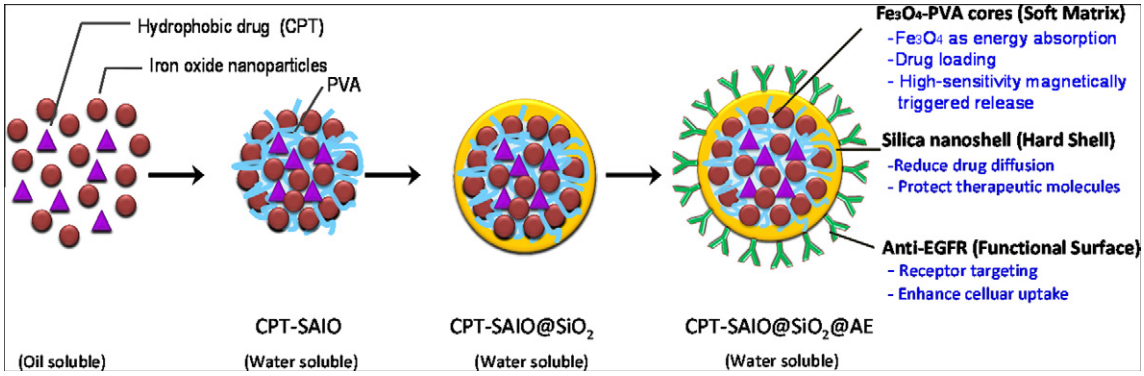

Fig. 3. Schematic illustration of the synthesis and structure of the self-assembled and anti-EGFR conjugated iron oxide/silica core–shell (SAIO@SiO_2@AE) nanocarriers.

achieved upon magnetic stimulus. From monitoring the drug release profile up to 24 h (Fig. 2c), it seems that the action of drug release could be terminated efficiently when the stimulus was removed. These results are explained collectively by: (a) magnetic-induced heating should affect dissolution of CPT in DMEM and enhance a corresponding release profile; (b) nanostructural disruption, especially the thin silica shell, may be transient, in other words, no permanent damage, but temporary deformation was operated upon the stimulus; and (c) such CPT-containing core–shell nanocarriers provide great advantages in managing sustained release with precise dose control in physiological conditions.

3.4. Preparation of ligand-modified CPT-SAIO@SiO_2 nanocarriers

To impart targeting capability further onto the CPT-SAIO@SiO_2 nanocarrier, the SAIO@SiO_2 nanocarriers were conjugated with the antibody, i.e. anti-EGFR, for active targeting purposes, which is illustrated schematically in Fig. 3. Upon modification, amino groups, exposed on the surface of the silica shell, were anchored chemically using APTMS under condensation reaction, then the amino groups conjugated to the anti-EGFR on its carboxyl site using EDC as a linker (hereinafter, this is termed CPT-SAIO@SiO_2@AE nanocarrier). Since it has been well recognized that binding of ligands onto EGFR can stimulate cell growth; therefore, employing EGF as a targeting ligand onto a drug carrier is expected to influence cellular behaviors, including cell growth (because EGF mediates cellular signals), cell proliferation/differentiation, cell cycle progression, adhesion, invasion, angiogenesis and inhibition of apoptosis [31,32]. However, to avoid the interference arising from cell growth and proliferation, neutralization of anti-EGFR antibody is also selectively employed in this study. The coupling efficiency of anti-EGFR on the nanocarriers was determined by UV–Vis spectroscopy at 275 nm, which gave ~75% of the added anti-EGF

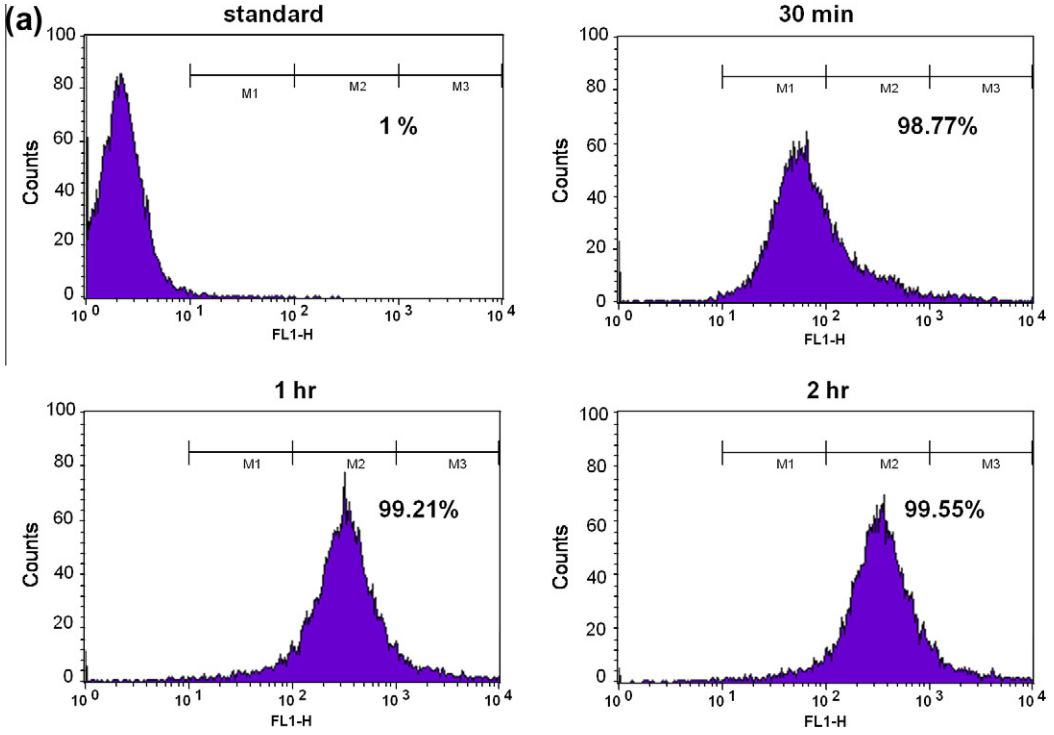

Fig. 4. Cell uptake efficiency measured by flow cytometry analysis for the FITC-SAIO@SiO_2@AE nanocarriers accumulated in A549 (a) for periods of time; and (b), (c) comparison of cell uptake efficiency and proportion of fluorescence intensity of SAIO@SiO_2@AE and SAIO@SiO_2 nanocarriers. (d) SAIO@SiO_2@AE nanocarriers accumulated in MCF7 cells for 1 h.

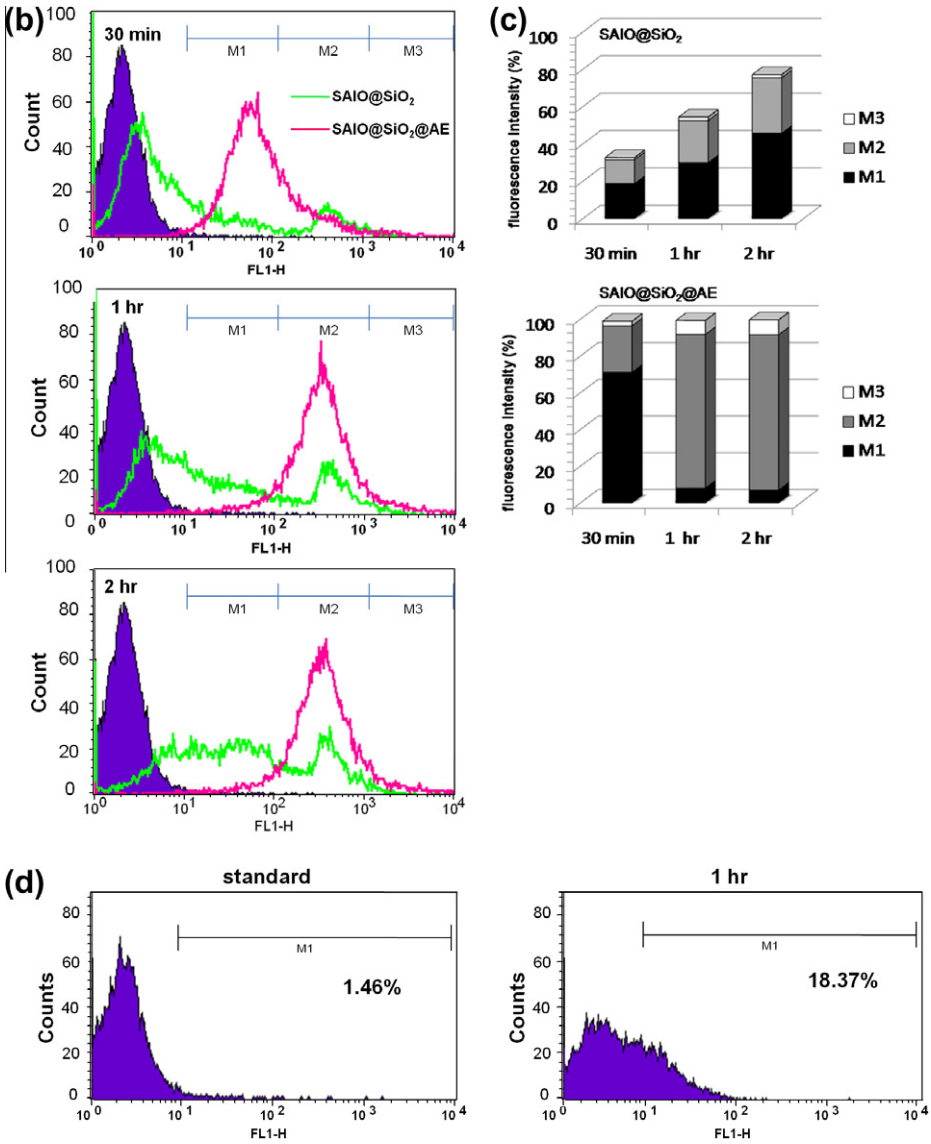

Fig. 4 (*continued*)

coupled with the CPT-SAIO@SiO_2 nanocarriers, which corresponds to ~7.5 μg anti-EGFR on the surface of 1 mg CPT-SAIO@SiO_2 nanocarriers.

3.5. Selective cellular uptake

EGFR is known to be overexpressed in a variety of human carcinomas, including cancers at the sites of head and neck, breast, colon, ovary, lung, prostate and liver [33,34]. Enhanced EGFR expression is associated with tumor invasiveness and resistance to chemotherapy and radiation therapy, and correlates clinically with poor prognosis and lower patient survival. A549, a cell line from non-small cell lung cancer, has been reported with EGFR overexpression, as detected by immunohistochemistry, and also plays an important role in tumor formation and progression. With such a characteristic of the A549 cell, the CPT-SAIO@SiO_2@AE nanocarriers were then employed for targeting evaluation.

The CPT-SAIO@SiO_2@AE nanocarriers were internalized into the A549 cells efficiently within 30 min, as characterized using fluorescence microscopy, and were monitored quantitatively by flow cytometry. Fig. 4a shows the flow cytometric spectra of the CPT-SAIO@SiO_2@AE nanocarriers which were subjected to the cells with an exposure time varying from 30 min to 2 h. Though the proportional amount of the nanocarriers taken by the cells (M1 + M2 + M3) was very much the same over periods of 30 min, 1 h and 2 h, corresponding to 98.77%, 99.21% and 99.55%, respectively, the peak showed a pronounced right shift, i.e. when treated with FITC-labeled CPT-SAIO@SiO_2@AE nanocarriers for 30 min, the fluorescence spectra of A549 cell were localized between ~$10^1$and 10^2, and accumulated between ~10^2 and 10^3 for a 2-h period. The corresponding fluorescence intensity was increased as measured by FACS, which suggests an increasing amount of the CPT-SAIO@SiO_2@AE nanocarriers being taken by a single cell. By comparison with the CPT-SAIO@SiO_2 nanocarriers incubated with A549 for various time periods, as shown in Fig. 4b and c, the A549 cells took the CPT-SAIO@SiO_2@AE nanocarriers in a much more efficient way. Such an outcome strongly implies EGFR overexpression on A549 cell membrane, and the anti-EGFR could bind efficiently to A549 cells and consequently enhanced cell uptake efficiency. Further analysis of the flow cytometric spectra indicates that the fluorescence intensity distribution of cells subjected to CPT-SAIO@SiO_2@AE nanocarriers shows more agglomeration than that

subjected to CPT-SAIO@SiO_2 nanocarriers, where the spectrum of the fluorescence intensity for the cells treated with CPT-SAIO@SiO_2 nanocarrier showed a broad distribution, which was interpreted as each cell taking a different number of CPT-SAIO@SiO_2 nanocarriers, as selectively illustrated in Fig. 4b, where the fluorescence intensity of cells illustrated a broad range of $\sim10^1$–10^2 (M1), $\sim10^2$–10^3 (M2) to $\sim10^3$–10^4 (M3).

However, upon accumulating and analyzing 10,000 events using the CPT-SAIO@SiO_2@AE nanocarriers, the fluorescence spectrum displayed similar intensity, i.e. the fluorescence intensity of cells agglomerated in M1 for incubating with CPT-SAIO@SiO_2@AE nanocarriers for 30 min, but mostly accumulated in M2 over the period between 1 and 2 h. Such a well-evolved spectral distribution suggests that each A549 cell is able to take in efficiently nearly the same and sufficient amounts of the CPT-SAIO@SiO_2@AE nanocarriers, making a uniform distribution of the CPT-SAIO@SiO_2@AE nanocarriers residing along with the A549 cells. However, in comparison with the CPT-SAIO@SiO_2@AE nanocarriers, the CPT-SAIO@SiO_2 nanocarriers seemed randomly taken into the cells, as also evidenced by corresponding fluorescence spectra, where a broad distribution of the CPT-SAIO@SiO_2 nanocarriers has been found from cell to cell. In other words, this finding suggests that some cells took a few of the CPT-SAIO@SiO_2 nanocarriers, while some took more. The rationale behind the big difference in the distribution of the CPT-SAIO@SiO_2 nanocarriers within the A549 cells is not clearly understood at present, but it may be related to the initial non-uniform dispersion of the CPT-SAIO@SiO_2 nanocarriers while mixed with DMEM in the cell-cultured well, associated with a poor uptake ability to the A549 cells, resulting in a wider CPT-SAIO@SiO_2 nanocarrier distribution among the A549 cells. However, what is more critical to this argument is that such a wide nanocarrier distribution among the cells may give rise to poorer therapeutic efficacy in clinical practice, if, when only a few nanocarriers are taken in the cells, a dose of drug being released in the cell which is too low to inhibit the proliferation and growth of A549 cells effectively. In contrast, a more uniform and sufficient loading of the CPT-SAIO@SiO_2@AE nanocarriers ensure enhanced therapeutic efficacy and will be elucidated in detail in the forthcoming analysis. Such a highly effective and uniform cell-uptaken phenotype of the CPT-SAIO@SiO_2@AE nanocarriers displayed great potential to develop as a novel nanoplatform in clinical applications as a result of their targeting and dosing accuracy, especially for anti-cancer therapy.

3.6. Targeting evaluation of the ligand-modified nanocarriers

A549 cells overexpressed EGFR on the cell surface; in contrast, MCF7, human breast cancer cells showed low EGFR on the cell membranes. As shown in the flow cytometric spectra in Fig. 4d, after a 1-h coincubation with the CPT-SAIO@SiO_2@AE nanocarriers, the MCF7 shows relatively poor cell uptake efficiency in comparison with that of the A549 cells (Fig. 4a). This finding suggests a potentially feasible strategy using cell-specific selectivity of the ligand-modified nanocarriers to cells with a specific nature of receptors on the cell membrane. A test was then designed, co-cultivating both cell lines in order to monitor the targeting capability of the CPT-SAIO@SiO_2@AE nanocarriers. The images (Fig. 5) from confocal microscopy strongly suggest that the CPT-SAIO@SiO_2@AE nanocarriers are largely and preferentially bound by the A549 cells over a 1-h duration of incubation, where the green particles were largely detected in A549 cells (as indicated by the arrow). These cellular images showed that the CPT-SAIO@SiO_2@AE nanocarrier is capable of serving as an efficient and highly target-specific drug delivery nanosystem to EGFR expressed cells. As expected, the anchored anti-EGFR ligand molecules on the surface of the CPT-SAIO@SiO_2@AE nanocarriers provide high cellular recognition to A549 cells, rather than MCF7 cells, lacking the specific receptor on its cell membrane for biological recognition of the designed nanocarriers. However, the mechanism underlying cellular uptake of the nanocarriers has to be clarified in detail in order that more critical biological information can be employed to reinforce further the design of a intracellular-based drug delivery nanosystem for enhanced cellular uptake efficiency and a precise cellular-based controlled release of drug for enhanced therapeutic efficacy.

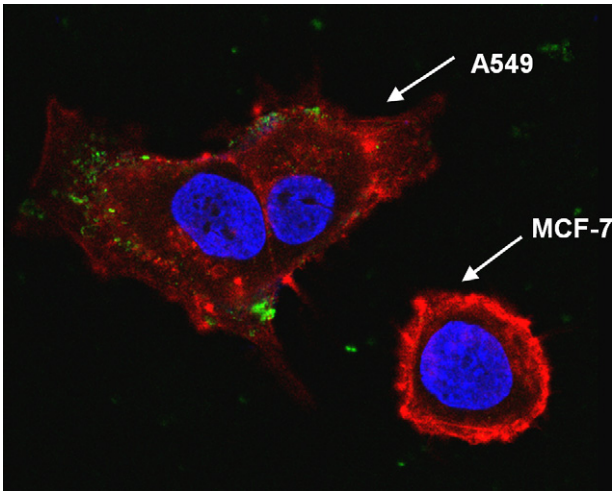

Fig. 5. Confocal microscopy images of CPT-SAIO@SiO_2@AE nanocarriers cultivated with a co-cultured (A549 and MCF7 cell) condition to monitor the targeting ability.

3.7. Endocytosis pathway identification

Since two kinds of nanocarriers, SAIO@SiO_2@AE and SAIO@SiO_2, showed different behavior of cell uptake, the different mechanism of internalization are thought to play an important role in such phenomena. Endocytosis is a multi-stepped complex cellular pathway for the internalization of ligands and/or macromolecules. To elucidate the endocytosis mechanism of the nanocarriers using the A549 cell as a model cellular system, various pharmacological inhibitors were used to explore the underlying endocytic mechanism. Inhibition of cellular uptake was performed in the presence of optimized single inhibitor concentrations of CytD (a macropinocytosis inhibitor), CPZ (a clathrin-mediated inhibitor), genistein

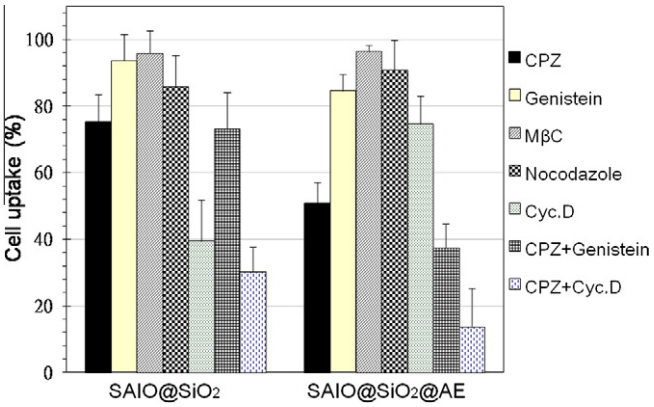

Fig. 6. Effects of endocytic inhibitors on the internalization of CPT-SAIO@SiO_2 and CPT-SAIO@SiO_2@AE nanocarriers. Cellular uptake (%) of nanocarriers was calculated by comparison with that in the absence of inhibitor (100%). A549 cells were seeded, incubated with inhibitors, and treated with nanocarriers for 2 h, and subsequently, harvested for analysis by flow cytometry.

(caveolae-mediated inhibitor) and MβC (a caveolae-mediated and caveolae- and clathrin-independent pathway inhibitor), nocodazole (a microtubule inhibitor) and with double and triple inhibitor combinations. The quantitative analysis of the cellular internalization of the nanocarriers was carried out by flow cytometry, and cellular uptake (%) on A549 was calculated by comparison with that in the absence of inhibitor (as 100% basis) for both CPT-SAIO@SiO_2 and CPT-SAIO@SiO_2@AE nanocarriers, as shown in Fig. 6. For the CPT-SAIO@SiO_2 nanocarriers, the pathway of cellular uptake was found to be associated with macropinocytosis, clathrin-mediated endocytosis, and probably microtubule action; for the CPT-SAIO@SiO_2@AE nanocarriers, cellular uptake pathway appeared to come through macropinocytosis, clathrin-mediated endocytosis, and a small portion of caveolae-mediated endocytosis. When treated with CytD, the efficiency of cellular uptake for the CPT-SAIO@SiO_2 nanocarriers was reduced to 39%; by contrast, the cellular uptake reached 74% for the CPT-SAIO@SiO_2@AE nanocarriers. However, following the treatment of CPZ, the cellular uptake for the CPT-SAIO@SiO_2 improved to as high as 75%, while it was reduced to 50% for the CPT-SAIO@SiO_2@AE nanocarriers. From the inhibition study, it is identifiable that these nanocarriers entered A549 cells by the pathways of both macropinocytosis and clathrin-mediated endocytosis. For the CPT-SAIO@SiO_2@AE nanocarriers, major pathways include clathrin-mediated endocytosis, together with a small portion from macropinocytosis. However, for the CPT-SAIO@SiO_2 nanocarrier, the pathways are mainly associated with macropinocytosis, together with a small portion through clathrin-mediated endocytosis.

Such a distinct difference in the cellular uptake mechanism between these two types of nanocarriers is believed to result from the surface conjugation of the ligands, i.e., anti-EGFR. Several studies in the literature indicated that, when ligands bind to EGFR, endocytosis of EGF receptor complexes can be accelerated through clathrin-coated pits [35]. A clathrin-mediated endocytosis pathway is initiated by a specific ligand–receptor interaction on the extracellular surface. Upon endocytosis, internalized nanoparticles

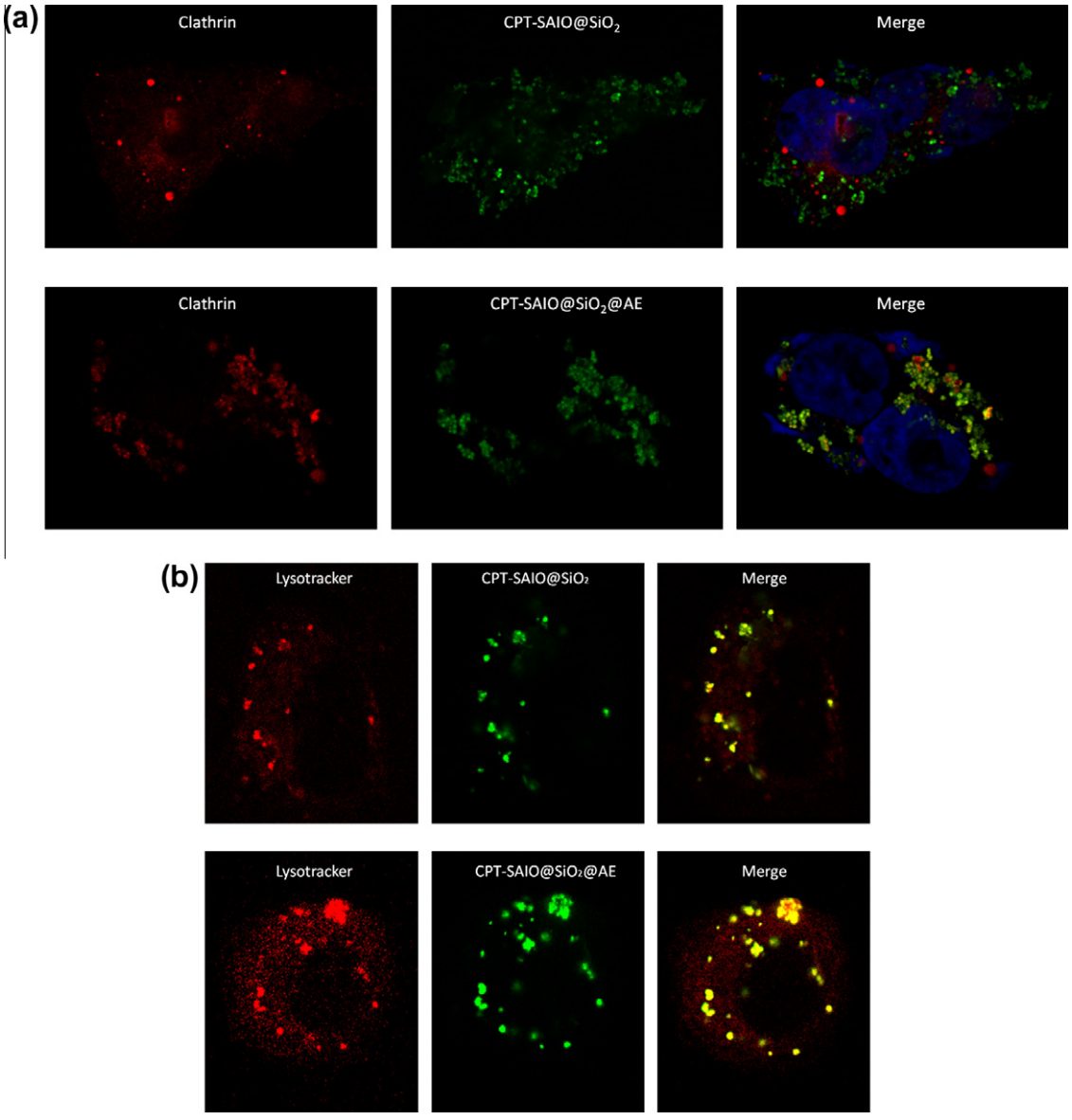

Fig. 7. Tracking fluorescein-labeled (a) CPT-SAIO@SiO_2 and CPT-SAIO@SiO_2@AE nanocarriers (green) in A549 cells. Additional staining of nuclei (DAPI-blue) and clathrin primary antibodies with secondary antibodies conjugated to Alexa Fluor 594 (red). (b) Colocalization of green fluorescent CPT-SAIO@SiO_2 and CPT-SAIO@SiO_2@AE nanocarriers with late endosomes/lysosomes with LysoTracker Red.

are generally entrapped in the intracellular vesicles (i.e. endosomes). Clathrin-mediated endocytosis has been recognized to be the fastest and highly regulated pathway of internalization of integral membrane proteins. The rapid cellular uptake efficiency of the CPT-SAIO@SiO_2@AE nanocarriers explained the pathway of clathrin-mediated endocytosis (Fig. 4). In addition, it may also induce pinocytosis when ligands bind to EGFR [36]. Together with the distinct difference in the distribution of the nanocarriers in A549 cells mentioned above, it can be concluded that clathrin-mediated endocytosis of the CPT-SAIO@SiO_2@AE nanocarriers ensures fast and uniform internalization compared with those, i.e. CPT-SAIO@-SiO_2 nanocarriers, without ligand modification. Moreover, particle size and shape are two of the important factors for the cellular membrane surface to recognize and eventually internalize through the cellular pathways [37], but this factor is unlikely to interfere with this investigation because the size and shape of both the CPT-SAIO@SiO_2 and CPT-SAIO@SiO_2@AE nanocarriers are nearly identical. Through FITC labeling, endocytosis of both the CPT-SAIO@SiO_2 and CPT-SAIO@SiO_2@AE nanocarriers entrapped into A549 cells was further substantiated by high-resolution confocal particle tracking to characterize the intracellular dynamics. The cells were incubated with primary antibodies against mouse clathrin (red fluorescence) after cell uptake. The immunofluorescence microscopic images showed that, as expected, FITC-loaded CPT-SAIO@SiO_2@AE nanocarriers were highly colocalized with clathrin (Fig. 7a); in contrast, less colocalization between FITC-labeled CPT-SAIO@SiO_2 nanocarriers and clathrin was observed. In addition, the nanocarriers also tracked to their intracellular trafficking fate by co-localization of LysoTracker Red where both CPT-SAIO@SiO_2 and CPT-SAIO@SiO_2@AE nanocarriers could be found in the late endosomes or lysosomes after internalization (Fig. 7b). The internalization pathway, as well as the intracellular fate of the nanocarrier, is a key issue for efficient drug delivery in the end. The release of the drug into the enzymatic environment of the lysosomes or directly into the cell cytoplasm will, indeed, have an important impact on the pharmacological activity.

3.8. Drug release from internalized nanocarriers via magnetic stimulus

Since a distinct difference in the pathway of cellular uptake for both the nanocarriers was observed experimentally and its effect on uptake efficiency and distribution in a single cell has been identified, it is more interesting to see whether such differences impart therapeutic efficacy while intracellular delivery of CPT via an external magnetic stimulus is performed. The CPT-SAIO@SiO_2@AE nanocarriers were prepared identically after 24-h incubation with A549 cells, following which the cell samples were placed into the coil of HFMF apparatus for a short-term magnetic stimulus of 30 s, 1 and 2 min, respectively. The temperature of the cultured wells was detected and found to be <40 °C for all the testing conditions. A control group with the CPT-free SAIO@SiO_2 nanoparticles was carried out under identical experimental protocol, showing constant cell viability (not shown), which ensures that the temperature effect (i.e. magnetic induced temperature rise) can be completely neglected in this study. The half maximal inhibitory concentration of CPT measured on A549 for 24-h incubation was ~200 ng ml^{-1}, and it was surprisingly to learn that the concentration turned only to ~39 ng ml^{-1} through treating with CPT-containing nanocarriers. In other words, to reach the same contributions in inhibiting the proliferation of A549 cells, the effective concentration of CPT was around five times less when CPT was loaded into magnetically sensitive CPT-SAIO@SiO_2@AE nanocarriers and released intracellularly. This finding also suggests that an enhanced therapeutic efficacy can be achieved if intracellular release of the drug can be performed precisely and efficiently. This further confirms the fact that the CPT-SAIO@SiO_2@AE nanocarriers displayed efficient inhibition of A549 cell proliferation, as illustrated in Fig. 8. This comes with a reasonable conclusion of rapid and high cellular uptake efficiency and uniform distribution in the quantity of the CPT-SAIO@SiO_2@AE nanocarriers internalized within A549 cells.

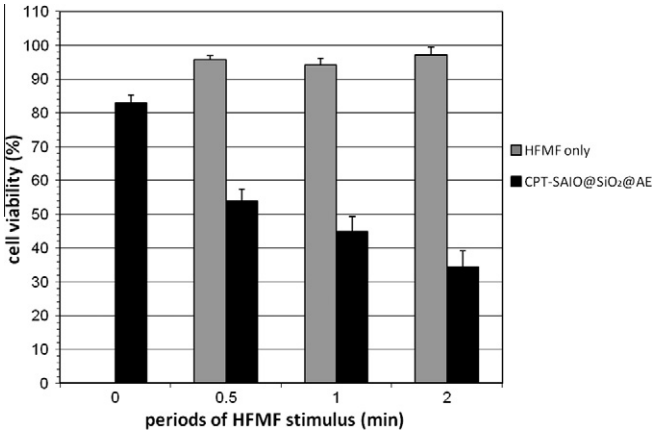

Fig. 8. CPT-SAIO@SiO_2@AE nanocarriers interacted with A549 cells for drug release from nanocarriers via HFMF stimulus. Cell viability of A549 incubated with CPT-SAIO@SiO_2@AE nanocarriers (100 μg ml^{-1}) or treated with HFMF for only 24 h. Cells were treated with nanocarriers for 6 h, and stimulated by HFMF for a period of 30 s, 1 or 2 min, then kept incubating for 18 h. Then the anticancer effect was measured by MTT assay. There is no influence on cell viability under HFMF only.

The CPT-SAIO@SiO_2@AE nanocarriers have clearly demonstrated an excellent targeted drug delivery system: not only its targeting capability by the EPR effect, but also high selectivity to EGFR overexpressed cells, which offered great potential in nanotherapeutic strategy and cytotoxic reduction compared with conventional chemotherapy using the same type of anti-cancer drugs. Moreover, a combined intracellular chemotherapy and thermotherapy can be highly manageable through the control of composition in the design of CPT-SAIO@SiO_2@AE nanocarriers and will be reported separately.

In conclusion, a core–shell multifunctional nanocarrier, namely CPT-SAIO@SiO_2@AE, with a magnetic iron oxide core and a silica shell capable of carrying anti-cancer drug (CPT), targeting EGFR overexpressed cancer cells, and precisely performing intracellular drug release, has been successfully designed, synthesized and systematically characterized in this work. Such nanocarriers showed reasonably high drug load efficiency toward CPT molecules, and high uptake efficiency to EGFR overexpressed cancer cells. The use of targeting moiety for functional modification of the nanocarrier ensures a rapid clathrin-mediated endocytosis toward A549 cell lines. Following the efficient pathway of cellular uptake, intracellular release of the CPT molecules via external magnetic stimulus has proved to be technically successful and ensures much higher therapeutic efficacy than that of the free drug. Cell culture study associated with a subsequent controlled drug release showed their outstanding potential in anti-cancer therapy as a result of their excellent and efficient cell-specific endocytosis and intracellular-based controlled drug delivery capability to cancerous cells. This work proved a successful and new therapeutic strategy by employing multiple functionalities to perform a cell-based nanotherapeutic treatment.

Acknowledgments

The authors thank Hong-Wei Chen and Peter Gout, Vancouver General Hospital and BC Cancer Research Centre, Canada, for fruitful discussion on the subject of cancerous cell biology and language

assistance with this manuscript, and also acknowledge the financial support of the National Science Council, Taiwan, NSC-98/99-2113-M-009-004.

Appendix A. Figures with essential colour discrimination

Figs. 2–7, are difficult to interpret in black and white. The full colour images can be found in the on-line version, at doi:10.1016/j.actbio.2011.03.021.

Appendix B. Supplementary data

Supplementary data associated with this article can be found, in the online version, at doi:10.1016/j.actbio.2011.03.021.

References

[1] Hans ML, Lowman AM. Biodegradable nanoparticles for drug delivery and targeting. Curr Opin Solid State Mater Sci 2002;6:319–27.
[2] Woodle MC. Sterically stabilized liposome therapeutics. Adv Drug Deliv Rev 1995;16:249–65.
[3] Farokhzad OC, Langer R. Impact of nanotechnology on drug delivery. ACS NANO 2009;3:16–20.
[4] Tan W, Jiang BS, Zhang Y. Quantum-dot based nanoparticles for targeted silencing of HER2/neu gene via RNA interference. Biomaterials 2007;28:1565–71.
[5] Yang T, Choi MK, Cui FD, Kim JS, Chung SJ, Shim CK, et al. Preparation and evaluation of paclitaxel loaded PEGylated immunoliposome. J Controlled Release 2007;120:169–77.
[6] Kirpotin DB, Drummond DC, Shao Y, Shalaby MR, Hong KL, Nielsen UB, et al. Antibody targeting of long-circulating lipidic nanoparticles does not increase tumor localization but does increase internalization in animal models. Cancer Res 2006;66:6732–40.
[7] Lu Y, Sega JE, Leamon CP, Low PS. Folate receptor-targeted immunotherapy of cancer: mechanism and therapeutic potential. Adv Drug Deliv Rev 2004;56:1161–76.
[8] Chen TJ, Cheng TH, Hung YC, Lin KT, Liu GC, Wang YM. Targeted folic acid–PEG nanoparticles for noninvasive imaging of folate receptor by MRI. J Biomed Mater Res Part A 2008;87A:165–75.
[9] Rosenholm JM, Meinander A, Peuhu E, Niemi R, Eriksson JE, Sahlgren C, et al. Targeting of porous hybrid silica nanoparticles to cancer cells. ACS NANO 2009;3:197–206.
[10] Duncan R. The dawning era of polymer therapeutics. Nat Rev Drug Discovery 2003;2:347–60.
[11] Matsumura Y, Maeda H. A new concept for macromolecular therapeutics in cancer chemotherapy: mechanism of tumoritropic accumulation of proteins and the antitumor agent smancs. Cancer Res 1986;6:6387–92.
[12] Moghimi SM, Hunter AC, Murray JC. Long-circulating and target-specific nanoparticles: theory to practice. Pharmacol Rev 2001;53:283–318.
[13] Gindy ME, Prud'homme RK. Multifunctional nanoparticles for imaging, delivery and targeting in cancer therapy. Expert Opin Drug Deliv 2009;6:865–78.
[14] Hu SH, Chen SY, Liu DM, Hsiao CS. Core/single-crystal-shell nanospheres for controlled drug release via a magnetically triggered rupturing mechanism. Adv Mater 2008;20:2690–5.
[15] Namiki Y, Namiki T, Yoshida H, Ishii Y, Tsubota A, Koido S, et al. A novel magnetic crystal-lipid nanostructure for magnetically guided in vivo gene delivery. Nat Nanotechnol 2009;4:598–606.
[16] Neuberger T, Schöpf B, Hofmann H, Hofmann M, Rechenberg B. Superparamagnetic nanoparticles for biomedical applications: possibilities and limitations of a new drug delivery system. J Magn Magn Mater 2005;293:483–96.
[17] Yoon TJ, Kim JS, Kim BG, Yu KN, Cho MH, Lee JK. Multifunctional nanoparticles possessing a "magnetic motor effect" for drug or gene delivery. Angew Chem Int Ed 2005;44:1068–71.
[18] Koh I, Wang X, Varughese B, Isaacs L, Ehrman SH, English DS. Magnetic iron oxide nanoparticles for biorecognition: evaluation of surface coverage and activity. J Phys Chem B 2006;110:1553–8.
[19] Veiseh O, Sun C, Gunn J, Kohler N, Gabikian P, Lee D, et al. Optical and MRI multifunctional nanoprobe for targeting gliomas. Nano Lett 2005;5:1003–8.
[20] Lu CW, Hung Y, Hsiao JK, Yao M, Chung TH, Lin YS, et al. Bifunctional magnetic silica nanoparticles for highly efficient human stem cell labeling. Nano Lett 2007;7:149–54.
[21] Burghard T, Andreas J. Clinical applications of magnetic nanoparticles for hyperthermia. Int J Hypertherm 2008;24:467–74.
[22] Serra L, Doménechc J, Peppas N. Engineering design and molecular dynamics of mucoadhesive drug delivery systems as targeting agents. Eur J Pharm Biopharm 2009;71:519–28.
[23] Dausend J, Musyanovych A, Dass M, Walther P, Schrezenmeier H, Landfester K, et al. Uptake mechanism of oppositely charged fluorescent nanoparticles in HeLa cells. Macromol Biosci 2008;8:1135–43.
[24] Meng W, Parker TL, Kallinteri P, Walker DA, Higgins S, Hutcheon GA, et al. Uptake and metabolism of novel biodegradable poly(glycerol-adipate) nanoparticles in DAOY monolayer. J Controlled Release 2006;116:314–21.
[25] Chithrani BD, Ghazani AA, Chan WCW. Determining the size and shape dependence of gold nanoparticle uptake into mammalian cells. Nano Lett 2006;6:662–8.
[26] Hu SH, Liu DM, Tung WL, Liao CF, Chen SY. Surfactant-free, self-assembled PVA-iron oxide/silica core–shell nanocarriers for highly sensitive, magnetically controlled drug release and ultrahigh cancer cell uptake efficiency. Adv Funct Mater 2008;18:2946–55.
[27] Fahr A, Liu X. Drug delivery strategies for poorly water-soluble drugs. Expert Opin Drug Deliv 2007;4:403–16.
[28] Rusch V, Klimstra D, Venkatraman E, Pisters PWT, Langenfeid J, Dmitrovsky E. Overexpression of the epidermal growth factor receptor and its ligand transforming growth factor a is frequent in resectable non-small cell lung cancer but does not predict tumor progression. Clin Cancer Res 1997;3:515–22.
[29] Sun S, Zeng H, Robinson DB, Raoux S, Rice PM, Wang SX, et al. Monodisperse MFe_2O_4 (M =Fe, Co, Mn) nanoparticles. J Am Chem Soc 2004;126:273–9.
[30] Hu SH, Liu TY, Huang HY, Liu DM, Chen SY. Magnetic-sensitive silica nanospheres for controlled drug release. Langmuir 2008;24:239–44.
[31] Gibson S, Tu S, Oyer R, Anderson SM, Johnson GL. Epidermal growth factor protects epithelial cells against Fas-induced apoptosis. J Biol Chem 1999;274:17612–8.
[32] Jorissen RN, Walker F, Pouliot N, Garrett TP, Ward CW, Burgess AW. Epidermal growth factor receptor: mechanisms of activation and signaling. Exp Cell Res 2003;284:31–53.
[33] Roskoski R. The ErbB/HER receptor protein-tyrosine kinases and cancer. J Biochem Biophys Res Commun 2004;319:1–11.
[34] Salomon DS, Brandt R, Ciardiello F, Normanno N, Ciardiello F, Normanno N. Epidermal growth factor-related peptides and their receptors in human malignancies. Crit Rev Oncol Hematol 1995;19:183–232.
[35] Alexander S, Lai KG. Endocytosis and intracellular trafficking of ErbBs. Exp Cell Res 2009;315:683–96.
[36] Lai SK, Hida K, Man ST, Chen C, Machamer C, Schroer TA, et al. Privileged delivery of polymer nanoparticles to the perinuclear region of live cells via a non-clathrin, non-degradative pathway. Biomaterials 2007;28:2876–84.
[37] Chithrani BD, Chan WCW. Elucidating the mechanism of cellular uptake and removal of protein-coated gold nanoparticles of different sizes and shapes. Nano Lett 2007;7:1542–50.